Journal of Atmospheric and Oceanic Technology

Validation of the CLARA-A3 top-of-atmosphere radiative fluxes climate data record

--Manuscript Draft--

Manuscript Number:	JTECH-D-23-0065
Full Title:	Validation of the CLARA-A3 top-of-atmosphere radiative fluxes climate data record
Article Type:	Article
Corresponding Author:	Tom Akkermans Royal Meteorological Institute Belgium (RMIB) Brussels, BELGIUM
Corresponding Author's Institution:	Royal Meteorological Institute Belgium (RMIB)
First Author:	Tom Akkermans
Order of Authors:	Tom Akkermans
	Nicolas Clerbaux
Abstract:	The third edition of the CMSAF cLoud, Albedo and surface RAdiation dataset from AVHRR data (CLARA-A3) features for the first time top-of-atmosphere products Reflected Solar Flux (RSF) and Outgoing Longwave Radiation (OLR), which are presented and validated in this paper on their full time span (1979-2020), using CERES, HIRS, and ERA5 products as reference data. The RSF data record is relatively stable as its bias w.r.t. ERA5 remains within +/-2Wm-2 for most of the time. Deviations are predominantly caused by the absence of either a morning satellite or an afternoon satellite, which occurs mostly in the first decade of the record. The radiative impact of the Pinatubo volcanic eruption is estimated at 3Wm-2. The RSF processing error (regional uncertainty) correlates with the number of available satellites and their local observation time (i.e., orbital configuration), which is most optimal during 2002-2016 and results in a monthly Mean Absolute Bias (MAB) w.r.t. CERES of around 2Wm-2 (daily MAB of 5Wm-2). The OLR data record is found relatively stable w.r.t. both ERA5 and HIRS, except for the first two years. The OLR processing error is quantified with a daily (monthly) MAB of around 1.5 (3.5) Wm-2during 2000-2020. It is less sensitive to orbital configuration compared to RSF, but especially for the daily MAB there is still a lower performance (MAB +40%) during periods with only morning or only afternoon observations (1979-1987). Overall, validation results are satisfactory for this first release of TOA flux products in the CLARA-A product portfolio. p { margin-bottom: 0.25cm; line-height: 115%; background: transparent }p.western { font-size: 12pt
Suggested Reviewers:	

Dr. Tom Akkermans and Dr. Nicolas Clerbaux
Ringlaan 3
1180 Brussels, Belgium
tom.akkermans@meteo.be
Tel.: +32 (0)2 373 05 50

Brussels, May 5th, 2023

Subject: submission of article to the Journal of Atmospheric and Oceanic Technology

Dear Editor,

I gladly present our draft article titled "*Validation of the CLARA-A3 top-of-atmosphere radiative fluxes climate data record*" for submission to the Journal of Atmospheric and Oceanic Technology (JTECH). The manuscript has not been previously published and is not currently under consideration by another journal.

The manuscript contains a presentation and thorough validation of the top-of-atmosphere radiative fluxes from the recently released CLARA-A3 data record, which bundles several products retrieved from the long-running AVHRR instrument record between 1979 and present.

The data record is developed by the EUMETSAT Climate Monitoring Satellite Application Facility (CMSAF) and is rigorously tested and validated before its release, like all CM SAF products. It was reviewed at several milestones in its development phase (requirements review, product consolidation review, delivery readiness review,..) with input from external independent reviewers. The documents generated during this process are published and available on the DOI landing page of the data record (https://doi.org/10.5676/EUM_SAF_CM/CLARA_AVHRR/V003). The "*CLARA-A3 Top-of-Atmosphere Radiation Validation Report*" on above mentioned web page (https://www.cmsaf.eu/SharedDocs/Literatur/document/2023/saf_cm_rmib_val_gac_toa_1_1_pdf) was used as basis to compile the submitted manuscript, which also explicitly refers to this document. During their review, it could be helpful for the reviewers to have this full validation report at hand, which contains much more details, is illustrated with more examples, and is written in a more elaborate style compared to the more concisely written submitted manuscript.

Yours sincerely,

The authors,
Tom Akkermans and Nicolas Clerbaux

Click here to access/download

Cost Estimation and Agreement Worksheet

Journals Estimation Worksheet TomAkkermans.pdf

Validation of the CLARA-A3 top-of-atmosphere radiative fluxes climate data record

Tom Akkermans,[a] and Nicolas Clerbaux[a]

[a] *Royal Meteorlogical Institute Belgium, Ringlaan 3, 1180 Brussels, Belgium*

Corresponding author: Tom Akkermans, tom.akkermans@meteo.be

ABSTRACT: The third edition of the CMSAF cLoud, Albedo and surface RAdiation dataset from AVHRR data (CLARA-A3) features for the first time top-of-atmosphere products Reflected Solar Flux (RSF) and Outgoing Longwave Radiation (OLR), which are presented and validated in this paper on their full time span (1979-2020), using CERES, HIRS, and ERA5 products as reference data. The RSF data record is relatively stable as its bias w.r.t. ERA5 remains within +/- 2 Wm^{-2} for most of the time. Deviations are predominantly caused by the absence of either a morning satellite or an afternoon satellite, which occurs mostly in the first decade of the record. The radiative impact of the Pinatubo volcanic eruption is estimated at 3 Wm^{-2}. The RSF processing error (regional uncertainty) correlates with the number of available satellites and their local observation time (i.e., orbital configuration), which is most optimal during 2002-2016 and results in a monthly Mean Absolute Bias (MAB) w.r.t. CERES of around 2 Wm^{-2} (daily MAB of 5 Wm^{-2}). The OLR data record is found relatively stable w.r.t. both ERA5 and HIRS, except for the first two years. The OLR processing error is quantified with a daily (monthly) MAB of around 1.5 (3.5) Wm^{-2} during 2000-2020. It is less sensitive to orbital configuration compared to RSF, but especially for the daily MAB there is still a lower performance (MAB +40%) during periods with only morning or only afternoon observations (1979-1987). Overall, validation results are satisfactory for this first release of TOA flux products in the CLARA-A product portfolio.

1. Introduction

Broadband top-of-atmosphere (TOA) Outgoing Longwave Radiation (OLR) and Reflected Solar Flux (RSF) are essential climate variables of which high-quality data records of satellite measurements with sufficient length ("Climate Data Record" or CDR) are needed by, among others, the climate modeling and climate monitoring communities, preferably spanning several decades.

To this end, three main approaches have been proposed and implemented: A first approach consists in dedicated ERB missions with broadband (BB) radiometers providing integrated observations of the radiation over large parts of the electromagnetic spectrum: "shortwave" (0.3–4μm) and "longwave" (4–50μm). A second approach consists in radiative transfer calculations based on cloud observations and atmospheric reanalysis. As a third approach, a so-called narrowband-to-broadband conversion can be used to directly estimate broadband TOA radiation from narrowband weather satellite observations taken at different wavelengths in the spectrum (visible and infrared).

Using this third approach, new RSF and OLR data records are generated as part of the third edition of the CM SAF Cloud, Albedo And Surface Radiation dataset from AVHRR data (CLARA-A3, Karlsson et al. (2023a,b)), featuring a fine spatial resolution (0.25°x0.25°) and long time span (42 years). The first and second CLARA editions were described by Karlsson et al. (2013) and Karlsson et al. (2017), respectively, and did not yet include TOA radiative fluxes. The newly generated RSF and OLR data record's retrievals and processing chains are documented by Akkermans and Clerbaux (2021) for the RSF and Clerbaux et al. (2020) for the OLR, each also including a preliminary validation on a limited amount of generated data.

This paper presents and validates the RSF and OLR data records on their full time span (1979-2020). This is done primarily by comparing with reference data records of proven quality and accuracy, but with shorter time span and/or coarser spatial resolution. Section 2 provides an overview of the different reference data records used for intercomparison. Section 3 describes the validation method, including the terminology, the applied statistical metrics, the data visualisation, and the temporally varying orbital configuration of the satellite constellation used to derive the CLARA-A3 data record. The validation results are presented and discussed in Sections 4 (RSF) and 5 (OLR), each describing the stability as well as the regional uncertainty of the data record. This is followed by Section 6 which provides a spatial view on the validation. Section 7 summarizes and concludes the paper, and offers an outlook for further research.

2. Reference data records used in the validation

a. CERES SYN1deg Ed.4.1 (daily and monthly)

The Clouds and Earth's Radiant Energy System (CERES, Wielicki et al. (1996)) product SYN1deg Ed4.1 provides estimates of the daily and monthly mean RSF and OLR fluxes from March 2000 onward at a 1°x1° lat-lon resolution. The products consist of CERES-observed (i.e. real broadband measurement), geostationary enhanced and temporally interpolated TOA radiative fluxes. Given the sun-synchronous orbits of the CERES instruments onboard the Aqua and Terra satellites, the observations are performed only twice a day. Therefore, hourly TOA fluxes and cloud properties from five contiguous geostationary imagers, covering 60°S–60°N at any given time, are used for an improved modelling of the diurnal variability between the CERES observations (Doelling et al. 2013). While the SYN1deg approach provides improved diurnal coverage by merging CERES and 1-hourly geostationary (GEO) data, artifacts in the GEO imager visible bands over certain regions and time periods can introduce larger regional uncertainties. Spurious jumps in the SW TOA flux record can occur when GEO satellites are replaced, because of changes in satellite position, calibration, visible sensor spectral response, cloud retrieval quality, and imaging schedules. Such artifacts in the GEO data can be problematic in studies of TOA radiation interannual variability and/or trends (Loeb et al. 2018). The issue does not play a role in the longwave product, given the general stability of GEO infrared bands due to onboard blackbody sources for calibration. In practice, CERES SYN1deg is still the best reference data record to validate daily TOA fluxes. It is used for the validation of daily and monthly global mean fluxes, from which the temporal variability determines the stability of the data record. It is used as well for the validation of processing error, containing the remaining random and systematic errors, which is performed at grid box level and therefore considered a validation of spatial patterns (also referred to as regional uncertainty), for which the SYN1deg product is suitable given its high spatiotemporal resolution (combination of GEO data). The largest disadvantage is the record's time span which is limited to 2000-2020, a period which is therefore referred to as the 'CERES era', in contrast to the period 1979-1999 ('pre-CERES era'). The data is downloaded from the 'CERES Ordering Tool' web portal (`https://ceres-tool.larc.nasa.gov/ord-tool/`). CERES products based on Terra and/or Aqua satellites suffer from data gaps in certain periods. As a consequence, three months are not used for validation purposes (August 2000, June 2001, March 2002). The impact of gaps after July 2002 is lower because since then the CERES products are composed of both Terra and Aqua satellite orbits.

b. CERES EBAF Ed.4.1 (monthly)

The CERES Energy Balanced and Filled (EBAF) Ed4.1 data record (Loeb et al. 2018) provides state-of-the-art estimates of monthly mean RSF and OLR fluxes from March 2000 onward at a 1°x1° lat-lon resolution. The longwave monthly mean EBAF product is computed directly from SYN1deg daily mean product, given the above mentioned stability of the GEO imager infrared bands. For the shortwave (SW) TOA fluxes, to maintain the diurnal information found in SYN1deg, but also preserve the excellent CERES instrument calibration stability (at their sun-synchronous observation times), the EBAF product introduced a new approach involving diurnal correction ratios (DCRs) to convert daily regional mean SSF1deg SW fluxes into diurnally complete values, analogous to SYN1deg but without geostationary artifacts (Loeb et al. 2018). Furthermore, even with the most recent CERES Ed4 instrument calibration improvements, the SYN1deg Ed4 net imbalance is still about 4.3 Wm^{-2}, much larger than the expected observed ocean heating rate of about 0.71 Wm^{-2} (Johnson et al. 2016). Therefore, the CERES EBAF dataset uses an objective constrainment algorithm (Loeb et al. 2009) to adjust SW and LW TOA fluxes within their ranges of uncertainty to remove the inconsistency between average global net TOA flux and heat storage in the Earth-climate system, mostly in the oceans. CERES EBAF is used for monthly global mean validation (stability) as well as for processing error validation (regional uncertainty). The record's time span is identical to the SYN1deg product, as is the record's download location (`https://ceres-tool.larc.nasa.gov/ord-tool/`).

c. HIRS OLR Daily v01r02

The NOAA National Centers for Environmental Information (NCEI) provides a high quality CDR of Outgoing Longwave Radiation (OLR) (Lee et al. 2007, 2014). Level-1b all-sky data from the High-resolution Infrared Radiation Sounder (HIRS) instrument are the main input into the daily OLR record. The data record is produced by applying a combination of statistical techniques, including OLR regression, instrument ambient temperature prediction coefficients and inter-satellite bias corrections. The HIRS OLR Daily data record is featured by a global coverage, a 1°x1° equal-angle grid resolution, and a temporal coverage from 1979 until present. The OLR estimated from imagers' radiance observations on-board operational geostationary satellites (via the Gridsat CDR and GSIP OLR product) is incorporated to allow an accurate temporal integration of the daily mean OLR. Since polar areas (about 60° polewards) are not covered by geostationary observations, only HIRS observations are used to derive the daily OLR in these regions. The HIRS OLR estimation technique has been vigorously validated against the Earth Radiation Budget Experiment (ERBE) and CERES data (Ellingson et al. 1994; Lee et al. 2007). The HIRS OLR Daily data record is in this paper used for daily and monthly global mean validation (stability), as well as for processing error validation (regional uncertainty) given its high spatiotemporal resolution (combination with GEO data). In contrast to the state-of-the-art CERES products, it's available for the entire time span of the CLARA-A3 record (1979-2020), making it the main reference data record for the OLR stability. In practice, it is used to verify whether the CERES performance is maintained backward in time, i.e. during the pre-CERES era. The monthly mean OLR is calculated by temporally aggregating the daily mean OLR. The data is downloaded from the 'UMD OLR CDR Portal' (`https://olr.umd.edu/`). In figures and tables, this reference data record is also referred to as "HIRS". A potential weakness of validating with HIRS is that it's derived using the same satellites (orbits) as the AVHRR instrument.

d. HIRS OLR Monthly v02r07

The HIRS OLR Monthly data record shares the same basic characteristics as the HIRS OLR Daily record, described in section 2c. The data record uses the Level-1b HIRS data as main input and is produced by applying the same combination of statistical techniques. However, the HIRS OLR Monthly time series is generated on a 2.5°x2.5° equal-angle grid. In addition, the monthly OLR CDR is estimated from the HIRS all-sky radiance observations directly and does not use geostationary observations, which results in a better temporal coverage (no data gaps due to unavailability of geostationary satellites). This data is used to address the stability of the monthly mean CLARA-A3 OLR products, but it is not used for regional validation because of its low resolution. The data have been downloaded from the 'UMD OLR CDR Portal' (`https://olr.umd.edu/`). In figures and tables, this reference data record is referred to as "HIRS-MM".

e. ERA5

ERA5 is the fifth atmospheric reanalysis from ECMWF (Hersbach et al. 2020). The data record provides a physically consistent blend of forecast and observations, resulting in a spatially and temporally seamless coverage. The model consists of the Integrated Forecasting System (IFS) cycle 41r2 with a 4-D variational analysis (4DVAR) assimilation system. The output has a temporal resolution of 1 hour, and a reduced gaussian spatial grid, which is bilinearly interpolated on a regular lat/lon grid of 0.25°x0.25°. The radiation scheme of ERA5 is described in Hogan and Bozzo (2018). The record's total time span is 1959-2020. Given the physical consistency throughout the record, ERA5 is selected for long-term global mean bias validation: it is useful to assess the stability of CLARA-A3's data record, especially when there is no other reference data record available, as is the case for RSF. On the other hand, ERA5 is a reanalysis product with a significant modeling component: it drastically underperforms in short-term spatially-explicit comparisons, making it not useful for processing error validation at regional scale. The data have been collected from the Copernicus Climate Data Store, available online at `https://cds.climate.copernicus.eu`.

f. ISCCP-FH and Cloud-CCI

The International Satellite Cloud Climatology Project FH product, or ISCCP-FH (Young et al. 2018; Zhang et al. 2019), is in essence a cloud product with TOA fluxes calculated from the retrieved cloud properties using a radiative transfer model (RadH-PRD). For the cloud retrievals, ISCCP-FH uses a composite of polar and geostationary satellites. The ISCCP FH data are provided on a 1°x1° lat-lon grid, and have been downloaded from `https://isccp.giss.nasa.gov/pub/flux-fh/tar-nc4_MPF/`.

Similar to ISCCP-FH, the Cloud-CCI data record (Stengel et al. 2020) is in essence a cloud product with TOA fluxes calculated from the retrieved cloud properties using the BUGSrad radiative transfer model. For the cloud retrievals, Cloud-CCI (L3C AVHRR-PM v3.0) is based purely on AVHRR afternoon satellites. The Cloud-CCI data are provided on a 0.5°x0.5° lat-lon grid and have been downloaded from `https://public.satproj.klima.dwd.de/data/ESA_Cloud_CCI/CLD_PRODUCTS/v3.0/L3C/`.

These products are only used to compare the global mean TOA flux (stability) with CLARA-A3 and other data records, and to make a brief assessment of their differences. They are not used for actual validation given their lower performance w.r.t. the state-of-the-art reference records CERES and HIRS.

3. Methodology

The three main uncertainty metrics discussed here are the mean bias, the stability, and the processing error (regional uncertainty) of the CLARA-A3 fluxes with respect to the reference data records.

a. Terminology

1) Mean Bias

The CLARA-A3 RSF and OLR products rely on empirical relations with CERES products, and hence their absolute radiometric level can be considered 'tuned' (not independent). Consequently, no attempt is done to quantify the metric in this paper. Rather than denoting the absolute radiometric error, the term 'Mean Bias' is here used to describe the daily mean overall bias with respect to a reference data record. It is calculated by subtracting the gridded CLARA-A3 flux from a gridded reference data record which produces a gridded bias (a 'bias map'), from which the global spatial average is taken. Depending on the reference data record, this Mean Bias may have several causes, such as a differences in calibration, satellite instruments, time of observation, temporal sampling, etc., which all have in common that they are not random but relatively constant in time and space (although they may slowly evolve in time, e.g. drifting of satellite orbit). Because of its tuned character, and given the significant regional bias variations (leading to large compensation effects), the Mean Bias itself is considered a less meaningful 'accuracy' metric for the CLARA-A3 TOA flux products. However, it is still interesting to compare the CLARA-A3 mean bias with other data records, i.e. how CLARA-A3 and these other data records are scaled compared to the absolute level of the CERES products.

2) Stability

The stability of the CLARA-A3 data record is evaluated as the maximum variation (max-min) of the global Mean Bias over a long time period (decades). A stable data record consists of a temporally systematic Mean Bias. Note that this stability is only relative to the inherent stability of the reference data record. Using different reference records allows attributing observed stability problems to one of these records. Variations or discontinuities, caused by several mechanisms mentioned above for the Mean Bias (section 3a.1), should remain within acceptable limits to render the data record useful for climate monitoring purposes.

3) Processing error (regional uncertainty)

The second source of uncertainty comes from the processing of AVHRR observations into TOA fluxes. This includes the conversion of the narrowband (channel) observations (reflectances and brightness temperatures) into broadband quantities, the subsequent integration from these directional to hemispherical quantities using Angular Dependency Models (ADMs), and finally the daily and monthly temporal interpolation of these quantities (see Akkermans and Clerbaux (2021) and Clerbaux et al. (2020) for details). To quantify this error, the CLARA-A3 products are compared with similar products derived from the CERES instruments at a 1°x1° spatial scale. CERES is considered as the best reference data to address this accuracy. For OLR, also HIRS is used to assess the processing error during the pre-CERES era (1979-1999). In practice, all data records are first regridded on the same nested 1°x1° lat-lon grid as used for the CERES products (see section 3b). Then, the bias-corrected mean absolute value of the difference with the CERES products is evaluated. It is interesting to look at time series of the processing error, to check the consistency over the data record extent, in particular to check that the errors obtained with different satellites (different AVHRR instruments) are consistent with each other. Even after correction for the global Mean Bias (section 3a.1), the processing error still contains a considerable regional systematic component: indeed, each grid box has a surface type which is generally invariant in time (e.g. ocean, desert, ..), and in some regions also the cloud cover has a preferential state (e.g. clear sky is dominant in the Sahara desert). Therefore, scene type dependent errors can be considered regionally systematic errors. This explains the "accuracy" part of the processing error. On the other hand, there is also a random component of the processing error. For instance, errors dependent on viewing and illumination geometry (angular dependent errors). For instantaneous fluxes, or for fluxes integrated on short time scales (e.g. daily mean), these errors can be significant. On longer time scales, for a given location (grid box), these errors cancel each other out since the angles of all observations are not constant but change randomly over time. Indeed, we see that a part of the processing error decreases when calculated on a longer time scale. This explains the “precision” part of the processing error, i.e. the random error. Accuracy and precision are therefore assessed together in the combined processing error, and globally integrated with the bias-corrected metric MAB, which is calculated spatially, i.e. over all the grid boxes, and for each time step (daily mean flux, monthly mean flux, ..). The processing error metric MAB is furthermore an expression of the regional uncertainty in the spatially-explicit grid of CLARA-A3 fluxes: it describes to which extent the bias deviates from its mean in the spatial dimension, i.e. how spatially homogeneous or heterogeneous the bias is (for a given temporal unit, i.e. for a given map depicting daily or monthly mean flux). The CLARA-A3 flux is provided with an uncertainty range of +/- MAB with 57.5% accuracy, assuming a Gaussian distribution.

b. Maps and grids

Unlike validation of global means, a spatially-explicit validation (such as MAB) requires each data record to be aggregated on a common base grid, typically the coarsest one. In this paper the coarse-resolution (2.5°x2.5°) HIRS-MM OLR Monthly v02r07 is not used for the spatially-explicit processing error analysis. All others data records were already available in (or were aggregated to) the so-called CERES Nested 1.0° grid (`https://ceres.larc.nasa.gov/data/general-product-info/#ceres-nested-10-processing-grid`), which was selected as common base grid.

Since this is an equal-angle grid, global statistical metrics (section 3c) would not represent the true spatial distribution as pixel area decreases poleward. Therefore, a meridionally varying weighting factor (w_j), which accounts for the spatial distortion, is applied to the statistical measures, thereby in practice converting the grid to an equal-area grid. The weighting factor is normalized so that its global average equals one.

c. Statistical measures

The retrieved daily mean CLARA-A3 flux (F_{CLARA}) is validated against the daily mean flux from a gridded reference data record, denoted by F_{REF}. The following statistical measures are used in the validation:

1) Bias defined per grid box ($B_{i,j}$)

Prior to the validation, the spatial resolutions of both F_{CLARA} and F_{REF} are first downgraded to match the CERES nested processing grid (section 3b). Maps of their difference are then created (daily "bias maps"), from which a single grid box with indices (i, j) is calculated as:

$$B_{i,j} = F_{CLARA,i,j} - F_{REF,i,j} \tag{1}$$

The grid box specific bias is used to calculate the other statistical measures.

2) Mean Bias (MB), defined globally

The global Mean Bias (MB) is calculated over all grid boxes' biases as follows:

$$\begin{aligned} MB &= \frac{1}{m \cdot n} \cdot \sum_{i=1}^{m} \sum_{j=1}^{n} w_j \cdot B_{i,j} \\ &= \frac{1}{m \cdot n} \cdot \sum_{i=1}^{m} \sum_{j=1}^{n} w_j (F_{CLARA,i,j} - F_{REF,i,j}) \end{aligned} \tag{2}$$

Where $B_{i,j}$ is the grid box specific bias, m and n are the number of grid boxes in longitude (360) and latitude (180) dimension, and w_j is a meridionally varying weighting factor to correct the equal-angle to an equal-area grid (see section 3b). The MB statistic is used in this paper to validate the stability of the global bias.

3) Mean Absolute Bias (MAB), bias-corrected, defined globally

The global Mean Absolute Bias (MAB) is calculated by first subtracting the global Mean Bias from every grid box' bias ($B_{i,j} - MB$), which corrects for the general bias. Subsequently, the absolute value is taken from the result, after which a global average is calculated in the same way as done for the global mean bias.

$$
\begin{aligned}
MAB &= \frac{1}{m \cdot n} \cdot \sum_{i=1}^{m} \sum_{j=1}^{n} w_j |B_{i,j} - MB| \\
&= \frac{1}{m \cdot n} \cdot \sum_{i=1}^{m} \sum_{j=1}^{n} w_j |F_{CLARA,i,j} - F_{REF,i,j} - MB|
\end{aligned} \tag{3}
$$

The MAB statistic is used in this paper to validate the processing error (regional uncertainty). Assuming normality, the range between +/-1 MAB contains roughly 57% of the data, and the range between +/- 2 MAB contains roughly 89% of the data.

d. Missing data and gap filling

Spatial and temporal gaps in CLARA-A3 are caused by a variety of reasons, discussed extensively in CMSAF (2022) (e.g. missing data in FDR, auxiliary input data,..). For specific periods, this may significantly impact the calculation of global mean values, leading to unrealistic time series of global mean TOA fluxes. This is avoided by filling these gaps with ERA5 fluxes, which have the advantage of full spatial and temporal coverage. Tests have shown that this gap-filling has very little effect on the validation results with bias and MAB (more details in CMSAF (2022)).

e. CLARA-A3 orbital configuration and temporal data visualization

The orbital constellation of AVHRR-carrying satellites is not constant but varies in time regarding the number of satellites, and regarding their respective local Equator Crossing Time (ECT). This is referred to as the "orbital configuration", which determines the temporal coverage of the observations throughout the day (density and spread of observations) for a given location. A single satellite observes a given location at the equator every 12 hours, i.e. two times per day (ascending and descending node), from which one during daylight conditions ('daytime') as illustrated in Figure 1 (useful for both RSF and OLR), and the other during nighttime, i.e. between 18h and 06h local time (only useful for OLR).

The satellites are launched on certain typical time slots, historically these are the morning orbit (around 7h30 ECT at launch) and the afternoon orbit (around 14h00-14h30 ECT at launch). Over time, they each tend to slowly drift towards the terminator, i.e. the morning orbit towards an

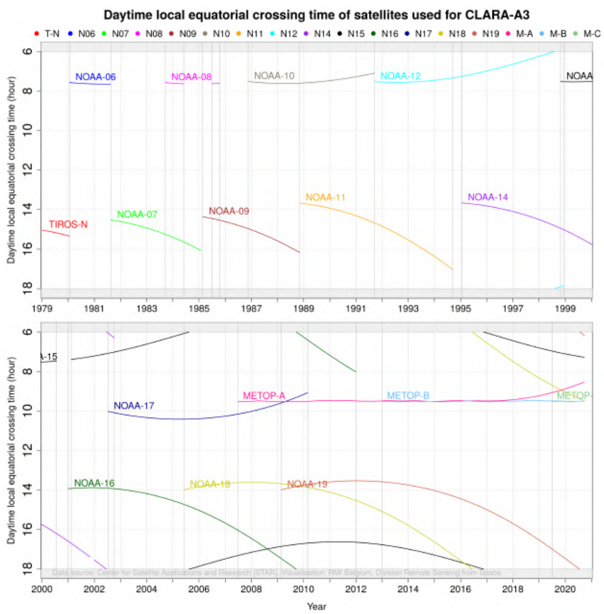

FIG. 1. Daytime local equator crossing time of satellites used for CLARA-A3

earlier ECT whereas the afternoon orbit towards a later ECT. It is worth mentioning here that this historical configuration was not symmetrical around noon (12h ECT), i.e. the morning orbit is always closer to the terminator compared to the afternoon orbit.

For some periods in the record, there is only one orbit available, either morning or afternoon. This limited temporal coverage is referred to as "suboptimal orbital configuration", as only a part of the day is covered. Note that it is not a binary issue: even in an orbital configuration with 2 satellites, the temporal coverage can be downgraded when one of the orbits has strongly drifted towards the terminator, thereby gradually resembling more and more a suboptimal orbital configuration.

The vertical solid gray lines in Figure 1 indicate transitions (discontinuities) in the orbital configuration, which often correspond to changes in (local) time of observation (i.e., ECT). These lines are included in all the temporal plots of this paper, and an overview of all these transitions is provided in Table 1.

4. Results for Reflected Solar Flux (RSF)

a. Mean bias and stability

As an illustration, the average CLARA-A3 RSF during 1979-2020 is shown in Figure 2.

Date (start)	Date (end)	Satellite(s)	Orbital configuration
1979-01-01	**1980-01-20**	**T-N**	**Aft. (=subopt.)**
1980-01-20	**1981-08-19**	**N-6**	**Mor. (=subopt.)**
1981-08-19	**1983-09-19**	**N-7**	**Aft. (=subopt.)**
1983-09-19	1984-06-01	N-8,-7	Mor., Aft.
1984-06-01	**1985-02-13**	**N-7**	**Aft. (=subopt.)**
1985-02-13	**1985-07-01**	**N-9**	**Aft. (=subopt.)**
1985-07-01	1985-10-14	N-8,-9	Mor., Aft.
1985-10-14	**1986-11-17**	**N-9**	**Aft. (=subopt.)**
1986-11-17	1988-11-08	N-10,-9	Mor., Aft.
1988-11-08	1991-09-16	N-10,-11	Mor., Aft.
1991-09-16	1994-09-13	N-12,-11	Mor., Aft.
1994-09-13	**1995-01-20**	**N-12**	**Mor. (=subopt.)**
1995-01-20	1998-10-26	N-12,-14	Mor., Aft.
1998-10-26	1998-12-14	N-15,-14,-12	Mor., Aft.
1998-12-14	2000-07-22	N-15,-14	Mor., Aft.
2000-07-22	**2001-01-01**	**N-14**	**Late Aft. (=subopt.)**
2001-01-01	**2001-02-12**	**N-16,-14**	**Aft. (=subopt.)**
2001-02-12	2002-07-11	N-15,-16,-14	Mor., Aft.
2002-07-11	2020-12-31	(multiple)	Mor., Mid-Mor., Aft.

TABLE 1. Transitions in CLARA-A3 orbital configuration; Abbreviations: T-N (Tiros-N), N-X (NOAA-X), Aft. (Afternoon), Mor. (Morning), subopt. (suboptimal).

Deseasonalized time series with global monthly mean RSF from different data records are shown in Figure 3, among which CLARA-A3 RSF in orange. Deseasonalization removes the mean annual cycle and hence also annually recurring biases, which is especially important for ERA5 RSF, as it is characterized by a significant bimodal seasonal bias (largely positive around December, moderately negative and positive around respectively April and June, and a largely negative around August; see CMSAF (2022), section 10.3); however, this only works well for systematic seasonal biases (i.e. occurring persistently during every year of the record) which is typically the case for model-based reanalyses such as ERA5. The deseasonalized ERA5 time series proves to be stable and can be used to assess the stability of other data records in the pre-CERES era (1979-1999). The two major volcanic eruptions El Chichón and Pinatubo are indicated on the time series, both having a radiative impact duration of about 21 months. El Chichón's radiative impact is estimated at +3 (CLARA-A3) and +2 (ERA5) Wm^{-2}, while Pinatubo's impact is estimated at +5 (CLARA-A3), +4 (ERA5) and +6 (ISCCP-FH) Wm^{-2}. The volcanic eruptions led to a dramatic increase in stratospheric sulfate

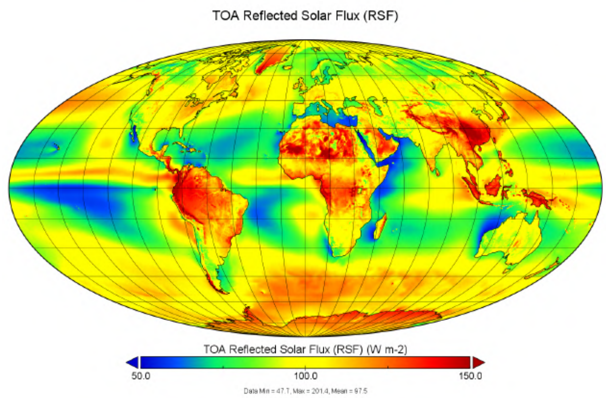

FIG. 2. Average CLARA-A3 RSF during 1979-2020

aerosol loading, causing a large rise in the reflection of solar radiation due to the optical properties of sulfuric acid droplets (Canty et al. 2013). Unlike the Pinatubo event, CLARA-A3 RSF does not properly capture the radiative impact of the El Chichón event: it features a temporary artificial drop of ~2 Wm^{-2} w.r.t. ERA5 during the impact event, around January 1983, Figure 3).

Global mean biases are calculated by subtracting the reference data records from CLARA-A3 RSF, resulting in the time series shown in Figure 4. The overall stability of CLARA-A3 RSF is assessed w.r.t. ERA5 (section 2e) by considering a so-called 'stability envelope' (target range), set symmetrically around the (slightly negative) mean of the bias, which is normally distributed (CMSAF 2022, section 5.1). The threshold requirement of 4 Wm^{-2} cited in CMSAF (2021, p.62-63) is selected as range for this envelope, and the overall stability remains within its limits for 94% of the time. During the CERES era (2000-2020) the CLARA-A3 RSF performance is very good, with a mean bias w.r.t. CERES SYN close to zero for the larger part of the two decades (red curve in Fig. 4). The largest bias fluctuations are situated in the first decade of the data record (until 1987), where the monthly RSF bias w.r.t. ERA5 (black curve) approaches or exceeds the edges of the stability envelope, but there are also some isolated peaks in later years (1994-'95, 1999, 2000). These biases are predominantly caused by CLARA-A3's "suboptimal orbital configuration" (section 3e): Incomplete temporal coverage of regional climate phenomena with an asymmetric diurnal cycle (e.g. marine stratocumulus thinning, land convection,..) introduces strong regional biases, from which the sign (positive or negative) depends on the region and observation time (morning, afternoon). Globally averaged, these biases vary seasonally because of the hemispherical imbalance of the associated regional climate feature's occurrence and strength.

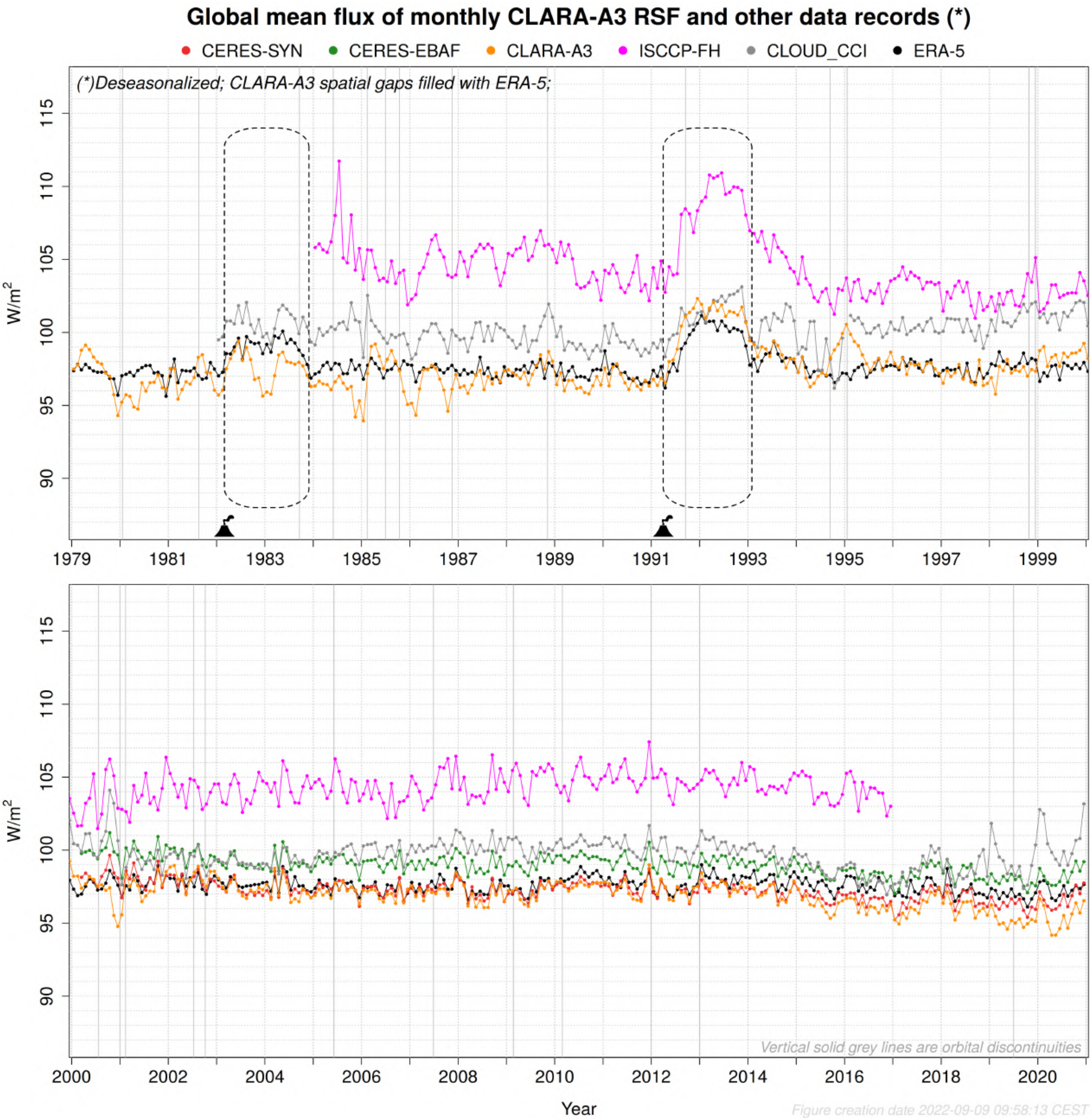

FIG. 3. Deseasonalized global mean flux of monthly CLARA-A3 RSF (in orange) and other data records.

As a result, it introduces a seasonally varying global mean bias during years with suboptimal orbital configuration (Table 1), which, in contrast to ERA5 biases, is not removed after deseasonalization, given its limited time span w.r.t. the entire data record's duration. The suboptimal configuration with only afternoon satellites (Table 1) is characterized by a unimodal seasonal bias (negative between November-February and positive between April-July), which causes the CLARA-A3 RSF

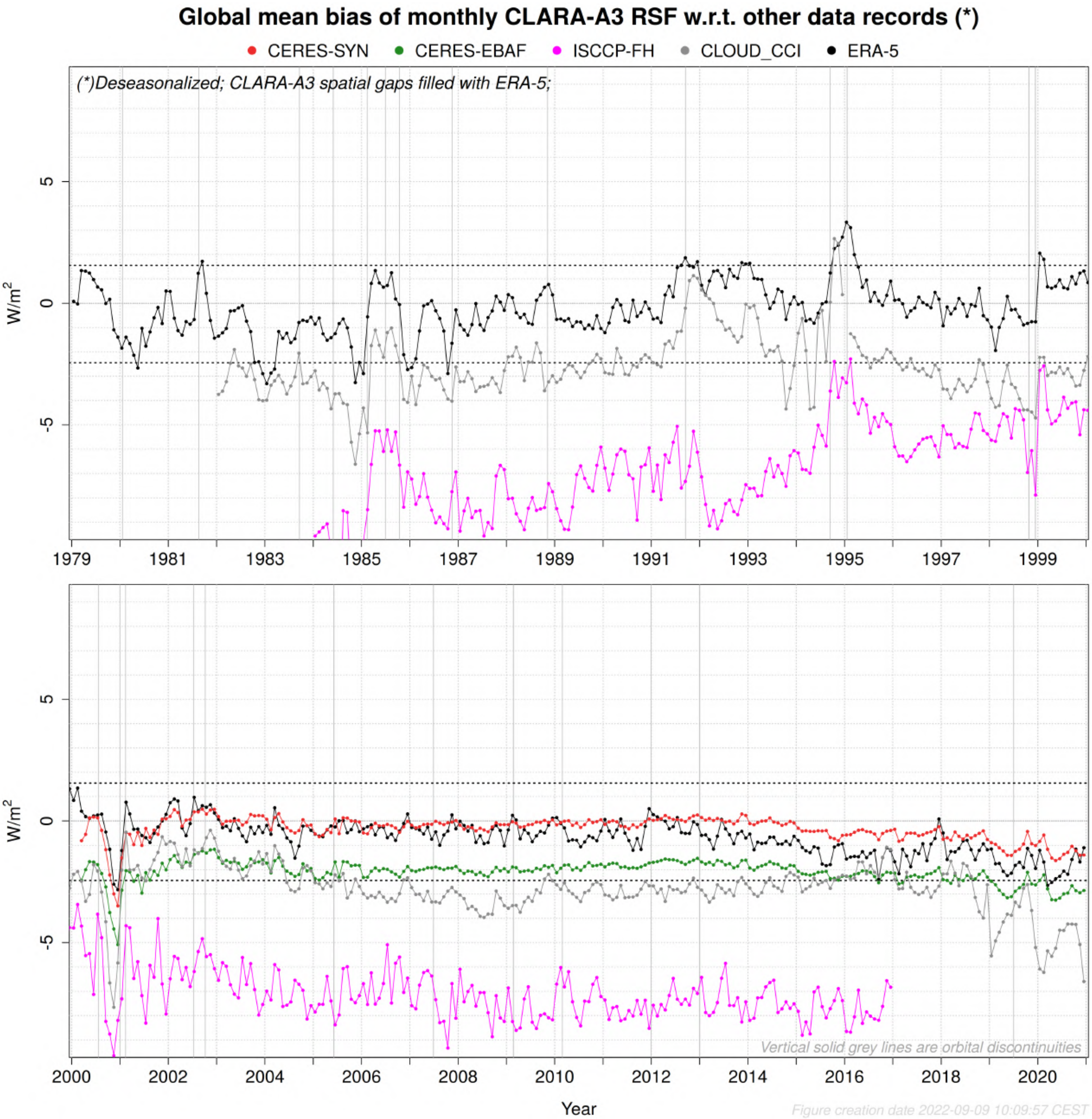

FIG. 4. Deseasonalized global mean bias of monthly CLARA-A3 RSF w.r.t. other data records. Dotted lines indicate a stability envelope of 4 Wm^{-2} around the bias w.r.t. ERA5.

radiative effect of the El Chichón event to be not well represented (cfr. the drop in CLARA-A3 RSF of about ∼2 Wm^{-2} w.r.t. ERA5 around January 1983 in Figures 3 and 4).

In the period of the Pinatubo eruption, between April 1991 and January 1993 (Figures 3 and 4), the bias between CLARA-A3 RSF and ERA5 increases by more than +1 Wm^{-2} compared to the period before and after. Here it probably concerns a bias in the ERA5 reanalyses, in which an underestimation of the prescribed aerosol optical depth would explain an underestimated RSF.

A slight downward trend in CLARA-A3 RSF of about -1 Wm^{-2} can be noticed between 2015-2020, which is caused by a trend in one of the satellites' Level-1 data record (Metop-B). It should be noted that MetOp-B was not well characterized because of its limited historic record when the FDR was generated. At that time, it was difficult to predict such a degradation and anticipate its future calibration parameters.

In absolute terms, it is not surprising that CLARA-A3 is close to CERES-SYN1deg (red curve in Figure 4) given the empirical relations between AVHRR and CERES that were first established offline (Akkermans and Clerbaux 2020) and then used to derive CERES-like broadband quantities in the data record's processing (Akkermans and Clerbaux 2021): this could be considered a kind of 'tuning' or 're-calibration' of the absolute radiometric level. More importantly, this time series is relatively flat which indicates a good stability w.r.t. the CERES products. The bias with CERES-EBAF is consistently ~1.5 Wm^{-2} lower (green curve in Figure 4), which can be explained by the EBAF adjustments made to comply with current estimates of the global energy imbalance. Similar to CLARA-A3 RSF, the Cloud-CCI data record is based on the AVHRR instrument, but the Cloud-CCI product shown in Figure 4 (in gray) is only based on afternoon satellites. Its overall stability is reasonable, mostly hovering around -2 to -3 Wm^{-2} w.r.t. CERES-SYN and CLARA-A3. Finally, the ISCCP-FH data record is considered the least performing, given its seemingly random and large short-term fluctuations (in the order of 2-3 Wm^{-2}) as well as long-term instability (oscillating between -10 and -5 Wm^{-2} w.r.t. CERES-SYN and CLARA-A3).

The daily mean analysis is not shown here, because the biases' magnitude and fluctuations are similar and are not affected by the temporal aggregation.

b. Processing error (regional uncertainty)

First the CERES era is discussed, i.e. the lower panel in Figure 5 (years 2000-2020). The months August 2000, June 2001 and March 2002 are not validated since the CERES products contain data gaps in those months, resulting in a total number of 247 months.

On average, the monthly MAB (w.r.t. CERES SYN1deg-Month) amounts 2.3 Wm^{-2} and the daily MAB (w.r.t. CERES SYN1deg-Day) amounts 6.2 Wm^{-2} (red curves in Figure 5). Much more than for the mean bias (section 4a), the processing error (regional uncertainty) during the CERES era is clearly related to the orbital configuration (Fig. 1). Best performance, with monthly and daily MAB around 2 and 5 Wm^{-2} respectively, is obtained with a maximum number and best spread of satellite observations throughout the day, i.e. best temporal coverage (2002-2016). The gradual decrease in performance (i.e. increase of MAB) after 2016 is due to orbital drift of the afternoon satellite towards an evening orbit (without introducing a new afternoon orbit with AVHRR instrument). The first years, until halfway 2002, are characterized by a markedly higher monthly and daily MAB, and again the main reason is the orbital configuration: indeed, the mid-morning orbit is only available since mid-2002. The sharp peak during the second half of 2000 represents the worst orbital configuration, being a single late afternoon orbit. The following distinct periods during the CERES era can be delineated, with MAB exhibiting large fluctuations with sharp delineations that are relatable to orbital configuration changes:

1. First half of 2000 with morning + late afternoon satellite: monthly and daily MAB of 4 and 10-13 Wm^{-2}, respectively
2. Second half of 2000 with a single late afternoon satellite (NOAA-14): monthly and daily MAB of 6-8 and 19-21 Wm^{-2}, respectively
3. Between 2001-mid2002 with morning + afternoon satellite: monthly and daily MAB of 2.5-3.5 and 8-10 Wm^{-2}, respectively
4. Between mid2002-2016 with mid-morning (NOAA-17) + afternoon satellite: monthly and daily MAB of 2 and 5 Wm^{-2}, respectively
5. After 2016 with midmorning and drifting afternoon satellite (NOAA-19): monthly MAB gradually increasing from 2 to 4 Wm^{-2} (monthly) and from 5 to 10 Wm^{-2} (daily)

A consistent seasonal cycle of the monthly MAB w.r.t. CERES EBAF is noticeable (green curve in Figure 5), contrary to the absence of such pattern in the MAB w.r.t. CERES SYN1deg (red curve), a discrepancy which is probably caused by a difference in the processing of CERES products. However, the latter is not entirely free from seasonality: the first and last few years of the MAB w.r.t. SYN1deg are also characterized by an increased seasonality (especially in the daily MAB), which is related to the above mentioned NOAA-19's orbital drift and the absence of NOAA-17's mid-morning orbit.

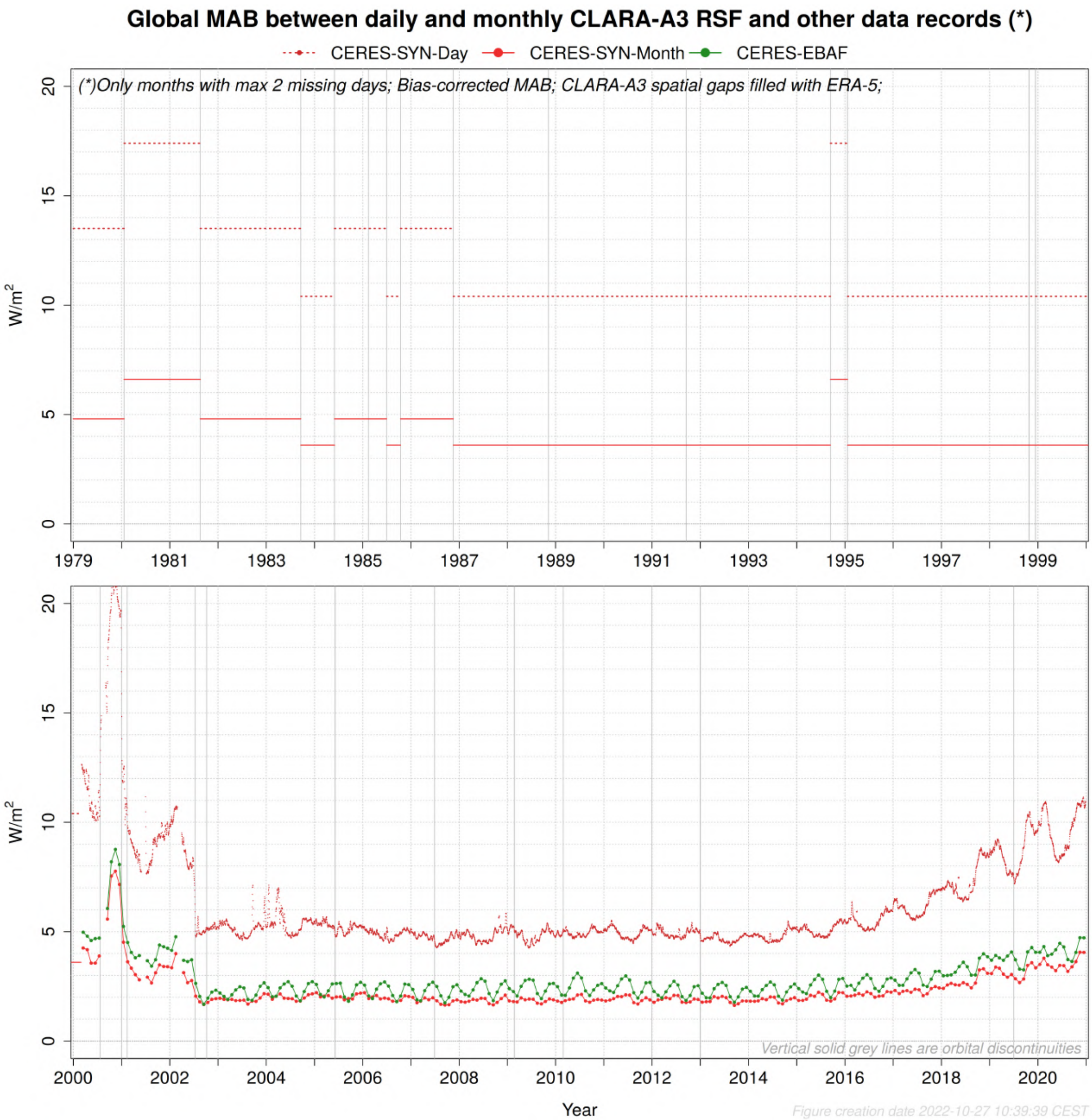

FIG. 5. Global MAB between daily and monthly CLARA-A3 RSF and other data records. Daily MAB is systematically higher than monthly MAB. The first half of the record are estimates of MAB calculated by mimicking three typical pre-CERES orbital configurations using equivalent (in terms of ECT) CERES-era satellites and time periods.

The increased MAB as well as its gradually increasing seasonality can both be explained by a degrading temporal coverage over regions characterized by large-scale regional climate phenomena with an asymmetric diurnal cycle (e.g. marine stratus thinning or land convection). This introduces strong regional biases, which can be positive or negative, depending on the region and kind of phenomena. Furthermore, a degrading temporal coverage also introduces strong biases with fast moving small-scale or heterogeneous weather systems (e.g. fronts), typically consisting of swirls with positive alongside negative bias, caused by an extrapolation of e.g. the mid-morning observation to the afternoon (when the afternoon satellite has disappeared or drifted toward the evening), or simply put: the weather moves too fast to be accurately observed (Akkermans et al., 2021). Globally averaged together, all these biases vary seasonally because of a hemispherical imbalance of the associated regional climate features' occurrence and strength, explaining the seasonal pattern of MAB. With any degradation of the temporal coverage (orbital configuration), such as NOAA-19's orbital drift, these regional biases grow accordingly, thereby directly increasing the global MAB (Fig.5). In contrast, the global mean bias is much less sensitive and remains relatively stable and without seasonal pattern during the CERES era (cfr. red curve in Fig. 4) because of compensating negative and positive regional biases. The bias is only affected with much worse temporal coverage, prevailing mainly during the pre-CERES era (suboptimal orbital configuration).

In addition, it is worth mentioning that observations with low illumination conditions (high solar zenith angle), prevalent close to the terminator, lead to a larger processing error, for instance due to the increased uncertainty of scene type defining parameters (cloud mask, cloud optical thickness, cloud phase,..) which propagates as uncertainty in the narrowband-to-broadband and ADM processes. This effect is also tied to the orbital configuration, as orbital drift typically increases the average solar zenith angle for a given location.

Besides the common overall characteristics and features of daily and monthly MAB, the daily MAB is generally higher compared to the monthly MAB. The reason is bias compensation, on different levels and scales. Firstly, there is a temporal sampling compensation: biases caused by fast moving small-scale or heterogeneous weather systems (e.g. broken cloud fields) vary in sign from day to day, depending on the weather system's morphology and movements (direction, timing, speed..). The aggregation to a monthly mean bias smooths out this daily variability. Secondly, there are numerous error sources related to the retrieval of instantaneous TOA albedo, which are propagated to the daily mean RSF (and the less satellite observations per day, the stronger this propagation). However, averaged over 30 days many of these errors tend to cancel each other out.

Examples are the errors related to the ADM (viewing and illumination geometry change every day, this in contrast to geostationary observations) and errors related to scene type identification such as cloud cover and cloud properties (relevant for ADM but also for narrowband-to-broadband conversion, etc). According to the terminology outlined in section 3a, these kind of compensating errors could for a large part be considered as the random component of the processing error ('precision part'), characterized by the daily MAB, whereas the errors that are still detected in the monthly MAB could be considered the processing error's systematic component ('accuracy part').

Until here the MAB validation only concerns the so-called CERES era (2000-2020), roughly corresponding to the second half of CLARA-A3's data record time span. The first half of the record does not have a suitable reference data record to estimate the regional uncertainty. However, since it is clear from the second half of the record that the orbital configuration explains most of the variability, it is possible to estimate the MAB during the pre-CERES era by mimicking three typical pre-CERES orbital configurations using equivalent (in terms of ECT) CERES-era satellites and time periods. Appendix A provides the details of this theoretical exercise, from which the results can be viewed in the top panel of Figure 5 (years 1979-1999). Daily MAB for the morning-only orbital configuration is estimated at 17.4 Wm^{-2}, whereas the afternoon-only configuration at only 13.5 Wm^{-2}. This difference is due to their temporal asymmetry around solar noon, i.e. the morning orbit being closer to the morning terminator than the afternoon orbit is from the evening terminator (see section 3e).

The result is that for the entire data record time span, the average monthly and daily MAB w.r.t. CERES-SYN1deg is estimated at 3.2 and 9.0 Wm^{-2}, respectively.

5. Results for Outgoing Longwave Radiation (OLR)

a. Mean bias and stability

The average CLARA-A3 OLR during 1979-2020 is shown in Figure 6.

The deseasonalized global monthly mean OLR from different data records is shown in Figure 7, among which CLARA-A3 OLR in orange. The HIRS and ERA5 data records are stable with respect to each other, increasing the confidence in their ability to serve as stability benchmark for the other data records. Volcanically induced aerosols also trap thermal radiation, but the longwave radiative impact is lower compared to the shortwave (Canty et al. 2013), shown in section 4a, so

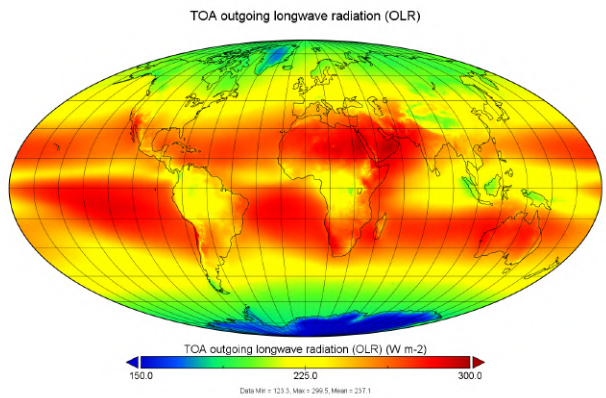

FIG. 6. Average CLARA-A3 OLR during 1979-2020

that the net effect is a climate cooling. The two major volcanic eruptions El Chichón and Pinatubo are indicated on the time series in Figure 7. The El Chichón eruption has no clear impact in the CLARA-A3 data record (but it might have caused a small drop of -0.5 Wm^{-2} in other data records), whereas the Pinatubo event probably caused a drop in OLR of approximately -1 Wm^{-2}, which is about half the assumed impact as seen in the HIRS OLR data records (-2 Wm^{-2}). Overall, for most data records these radiative impacts are almost similar to many other drops and jumps in the time series, making it difficult to assess and quantify them.

The global mean bias is calculated by subtracting the reference data records from CLARA-A3 OLR, resulting in the time series shown in Figure 8. The overall stability of CLARA-A3 OLR is assessed w.r.t. HIRS (section 2c), and similar to the RSF validation, this is done using a stability envelope with a range of 4 Wm^{-2} (i.e. the threshold requirement cited in CMSAF (2021, p.62-63)), which is arbitrarily set to [-3.2 ; +0.8] Wm^{-2} because the OLR bias is not normally distributed (figure not shown), as explained in CMSAF (2022, section 6.1). The overall stability remains within its limits for 99.6% of the time. The same results are obtained when assessing the stability with respect to HIRS-MM (section 2d). During the CERES era (2000-2020) the CLARA-A3 OLR performance is very good, with a relatively 'flat' mean bias w.r.t. CERES SYN, with an MAB between -1 and 0 Wm^{-2} for the larger part of the two decades. Note that CERES-EBAF is consistently ~1.5 Wm^{-2} lower (green curve in Figure 8), which is explained by the EBAF adjustments made to comply with current estimates of the global energy imbalance.

The first few years of the records are characterized by a distinctively more negative mean bias compared to the rest of the record. This period corresponds to coverage from the TIROS-N and

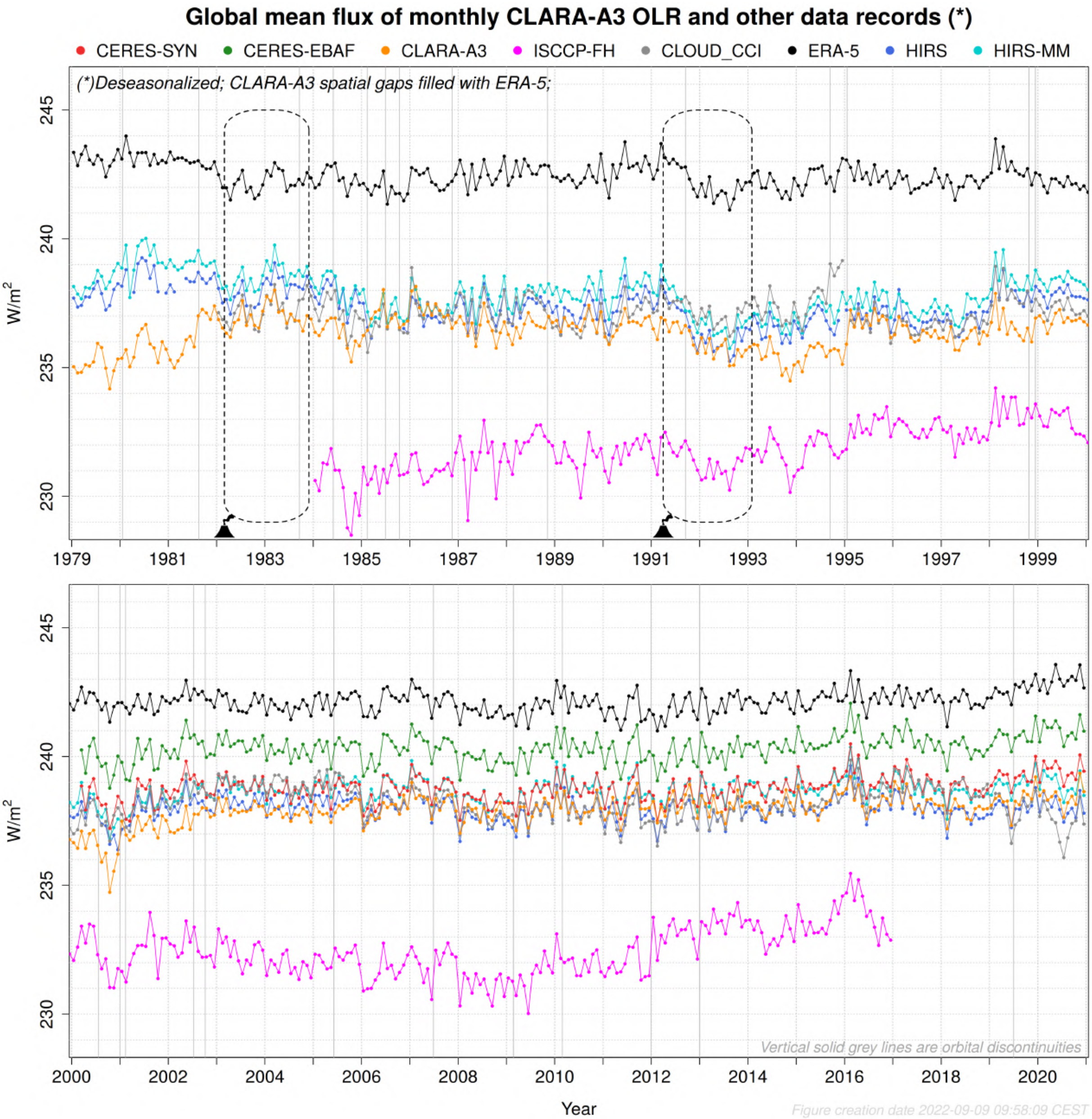

FIG. 7. Deseasonalized global mean flux of monthly CLARA-A3 OLR (in orange) and other data records.

NOAA-6 satellites (January 1979 - August 1981) and has an average bias of -2.5 Wm^{-2}, which is markedly lower than the mean bias between 1982-2002 (around -1 Wm^{-2}) and between 2002-2020 (around 0 Wm^{-2}). Additional investigations (analyses and figures not shown) exclude some potential factors as main cause (e.g. the morning-only orbital configuration, or the fact that early AVHRR instruments have only one thermal infrared channel), and indicate that the bias is likely due to an issue either with the calibration of the FDR or with the spectral response correction factors.

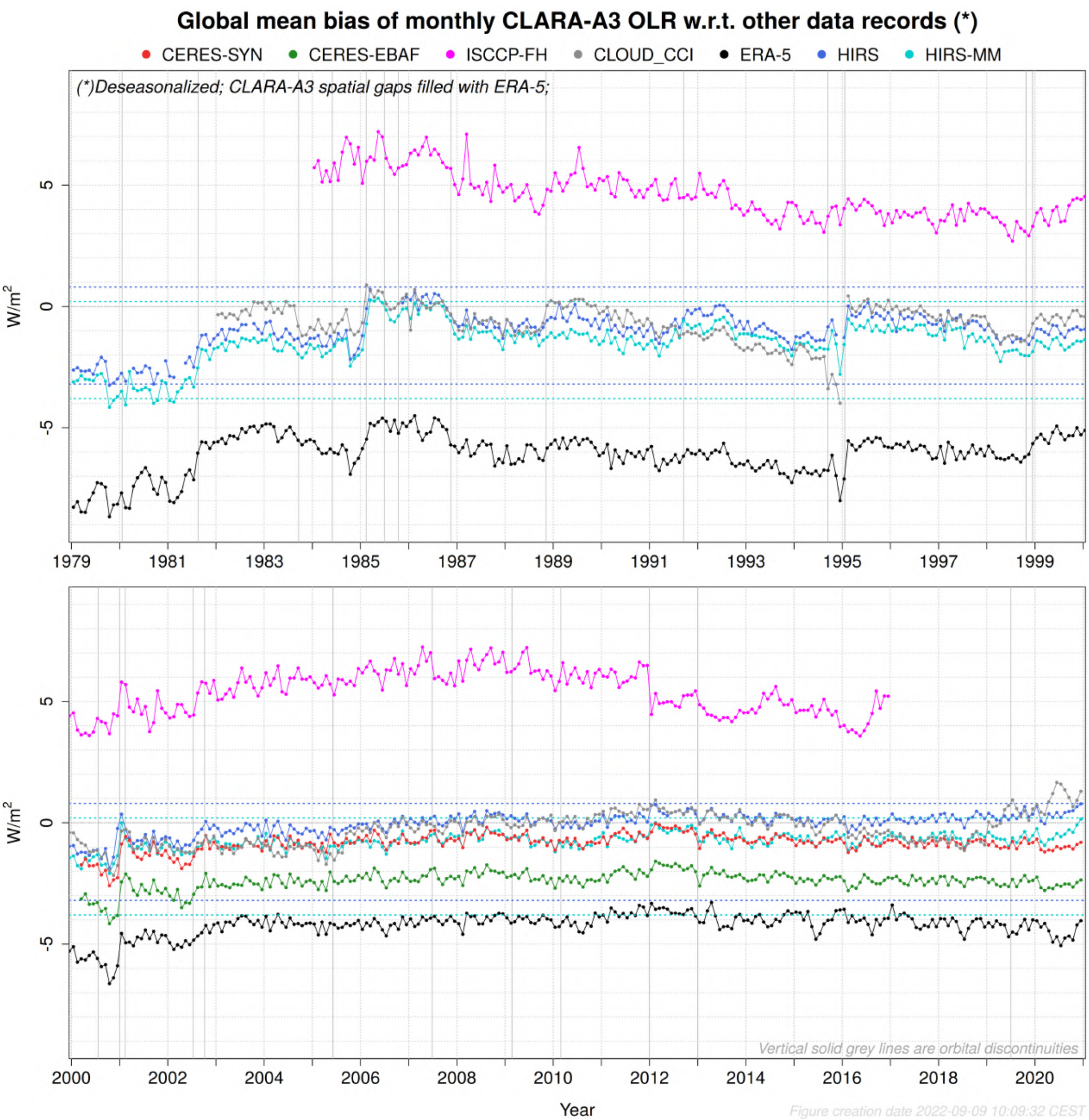

FIG. 8. Deseasonalized global mean bias of monthly CLARA-A3 OLR w.r.t. other data records. Dotted lines indicate a stability envelope of 4 Wm^{-2} around the bias w.r.t. HIRS.

The remaining first half of the record (1981-1999) is characterized by subtle patterns related to orbital configuration, most notably the gradual shift towards more negative biases with increasing ECT (orbital drift) marking distinct periods being 1985-1989, 1989-1994, and 1994-1999.

The daily mean analysis is not shown here, because the biases' magnitude and fluctuations are similar to the monthly results.

b. Processing error (regional uncertainty)

On average, the monthly and daily MAB w.r.t. HIRS (Fig. 9) amounts 1.8 Wm^{-2} and 4.8 Wm^{-2}, respectively. The daily MAB exhibits significant fluctuations with clear delineations that are relatable to changes in orbital configuration:

1. between 1979-mid1983 and mid1984-1986 with suboptimal orbital configurations, i.e. morning-only or afternoon-only satellite: daily MAB of 6-8 Wm^{-2};

2. the first half of 1984, and between 1987-2002, with mostly morning+afternoon satellites: daily MAB of 4-6 Wm^{-2}, slightly varying according to orbital drift;

3. distinct peaks during 1995 and 2000: with respectively an only-early-morning and an only-late-afternoon satellite: daily MAB of around 8 Wm^{-2};

4. between 2002-2016 with midmorning+afternoon satellites: daily MAB of 3.7 Wm^{-2}

5. after 2016 with midmorning + drifting afternoon satellite: daily MAB increasing to 4.5 Wm^{-2}.

Between April and October 1985 there are no valid HIRS observations, explaining the data gap in this period.

The underlying reasons for the dependency of OLR MAB on the orbital configuration are identical to the ones for RSF, as described in section 4b, however, the OLR is much less sensitive to it (compare Figures 5 and 9): the absence of the midmorning orbit NOAA-17 (before mid-2002) and the orbital drift of the afternoon orbit NOAA-19 (after 2016) both have only a small impact on OLR MAB (+0.5 to +1.0 Wm^{-2}), which is quasi constant between 2002-2016 (around 3.7 Wm^{-2}). Large degradations in orbital configurations have a bigger impact, for instance the late-afternoon-only configuration in the second half of 2000, causing the MAB to double (to 8 Wm^{-2}); however, these impacts are still small compared to RSF, where the same degradation leads to a quadrupling of MAB (Fig. 5). There are multiple reasons for this, for instance the intra-day relative range which is much lower for OLR than for RSF, thereby lowering the impact of wrong temporal extrapolation due to suboptimal temporal coverage. Another reason is the number of observations per day, which for OLR is double (compared to RSF) because it also relies on nighttime observations, which again lowers the impact of suboptimal temporal average on the daily mean integration.

In contrast to the daily MAB, the monthly MAB is even less sensitive to orbital configuration, for the same reasons as outlined in section 4b. It has a quasi constant MAB of around 1.5 Wm^{-2} between 2001-2020 (barely impacted by NOAA-19's orbital drift and absence of NOAA-17's midmorning orbit). On the other hand, large degradations in orbital configurations do have an impact, for instance the late-afternoon-only configuration in the second half of 2000, causing the MAB to increase to 2.5-3.0 Wm^{-2}; also here, these impacts are still small compared to the RSF, where the same degradation leads to a quadrupling of monthly MAB (Fig. 5).

6. Regional comparison (geographical distribution)

Although a regional analysis of the bias is beyond the scope of this paper, a bias map should provide basic confidence in its spatial distribution, for instance to verify that there are no problematic spatial differences. The 2000-2020 multi-annual mean of CLARA-A3 RSF bias w.r.t. CERES-SYN1deg is shown in Figure 10. The biases are generally relatively low in most regions (within +/- 2 Wm^{-2}), with some regions showing systematically (slightly) larger biases, in both negative sense (bluish colors; e.g. ocean west of African continent, Antarctica, eastern Canada,..) and positive sense (reddish colors; e.g. non-desert African and South-East Asian land masses), possibly related to specific scene types (snow/ice, tropical forest). Overall, however, the long-term averaged bias is considered acceptably low and sufficiently homogeneous.

The 1979-2020 multi-annual mean of CLARA-A3 OLR bias w.r.t. HIRS OLR is shown in Figure 11. The biases are generally relatively low in most regions (within +/- 2 Wm^{-2}), with almost no region-specific bias. Also here, the long-term averaged bias is considered acceptably low and sufficiently homogeneous.

7. Conclusions

This paper provides a first validation of the new CLARA-A3 TOA flux products, RSF and OLR, on their full temporal extent.

The CLARA-A3 Reflected Solar Flux data record is relatively stable as its bias w.r.t. ERA5 remains within +/- 2 Wm^{-2} for 94 % of the time. Deviations are predominantly caused by an incomplete temporal coverage (only morning or only afternoon orbit), which occurs mostly in the first decade of the record. The radiative impact of the Pinatubo volcanic eruption is estimated at

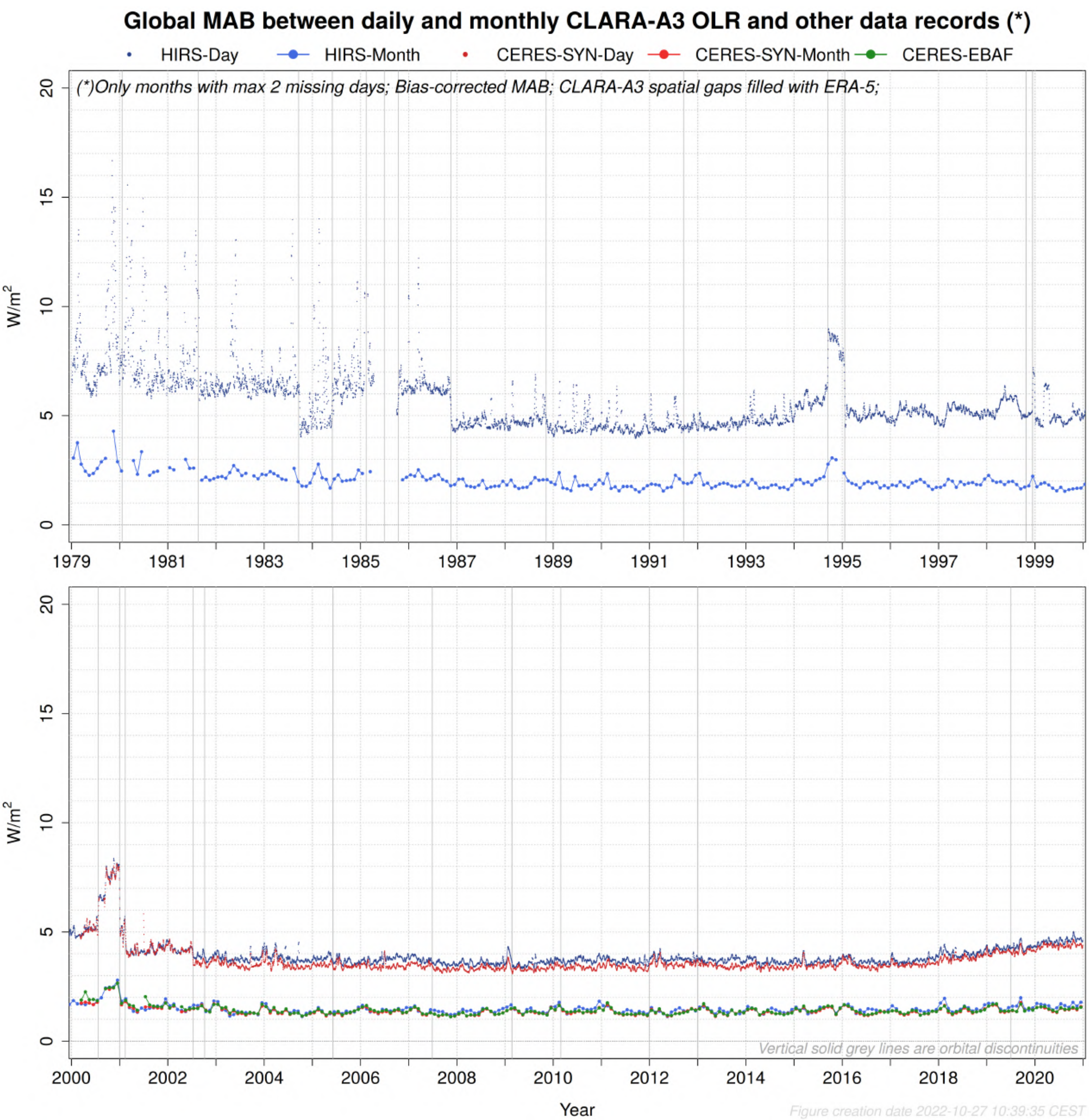

FIG. 9. Global MAB between daily and monthly CLARA-A3 OLR and other data records. Daily MAB is systematically 2-3 Wm^{-2} higher compared to monthly MAB.

3 Wm^{-2}. The RSF processing error (regional uncertainty) correlates with orbital configuration: best performance, around 2 Wm^{-2} for monthly MAB, is found with highest temporal coverage, i.e. number of contributing satellite orbits and spread in their overpass time, which is optimal during

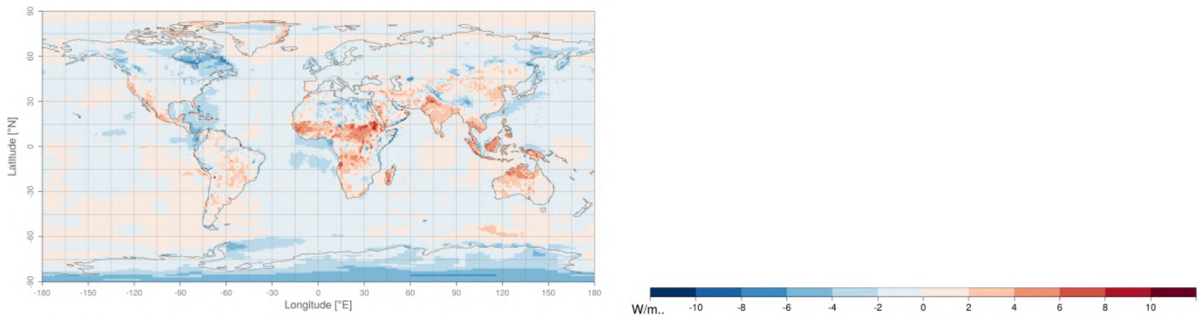

Fig. 10. Average RSF bias during 2000-2020 between CLARA-A3 and CERES-SYN1deg

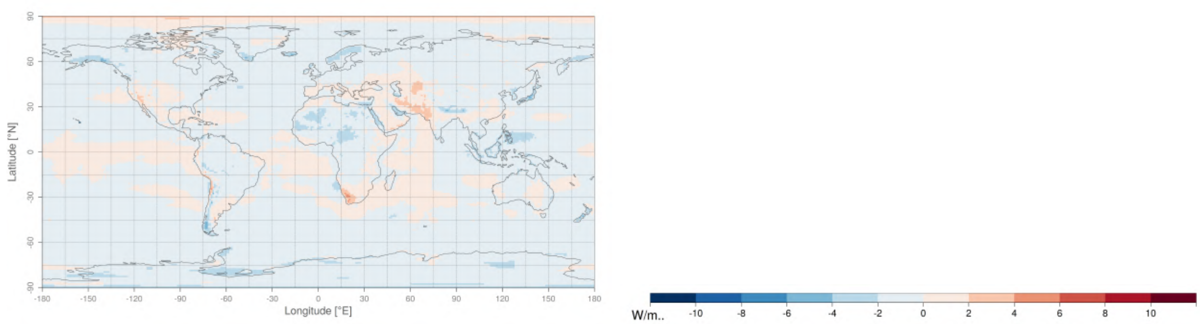

Fig. 11. Average OLR bias during 1979-2020 between CLARA-A3 and HIRS-OLR

2002-2016. Absence of the mid-morning orbit (before 2002) or early afternoon orbit (gradually after 2016) leads to a drop in performance (doubling of MAB).

The CLARA-A3 Outgoing Longwave Radiation data record is found relatively stable w.r.t. both ERA5 and the HIRS OLR data records, except for the first two years. Furthermore, orbital drift has a noticeable effect on the bias during the first half of the record (1979-1999). The OLR processing error is less sensitive to orbital configuration compared to RSF, but especially for the Daily MAB there is still a significantly lower performance (MAB +40%) for morning-only and afternoon-only orbits (1979-1987).

Overall, these validation results are satisfactory for the first edition of the flux products in the CLARA-A product portfolio. Uncertainties inherent to the polar orbiting satellite constellation are difficult to correct, especially for a constellation with persisting orbital drift, as is the case with most NOAA satellites; this in contrast to the CERES products, where the constant local observation time (equatorial overpass time) of the Aqua and Terra satellites allows for the development and implemention of a fixed instantaneous-to-diurnal correction. However, some potential improvements for future editions can be noted: (1) updating the currently implemented CERES Ed2 ADMs to the newest available CERES Ed4 ADMs could improve the instantaneous RSF estimation, as well as the albedo diurnal cycle models used to derive the daily mean flux. (2) the orbital drift effects of the last afternoon orbit (NOAA-19) could be solved by introducing orbits using a the VIIRS instrument, alongside the existing AVHRR-carrying orbits. (3) an update of the FDR with the newest calibration coefficients could solve calibration issues with the most recent satellites, such as MetOp-B and MetOp-C (and possibly also the two oldest, TIROS-N and NOAA-6).

The CLARA-A3 RSF and OLR products have unique properties, such as an unprecedented high resolution of 0.25° and almost double the time span of the current CERES data records. Another advantage is the flux product's synergy and compatibility with the other CLARA-A3 CDRs (cloud mask and other cloud parameters, surface radiation, surface albedo, etc.) sharing common algorithms and processing chains.

Acknowledgments. This work was funded by the Climate Monitoring Satellite Application Facility (CM SAF) of EUMETSAT. The authors are grateful to the Atmospheric Science Data Center at NASA Langley Research Center for providing the CERES data used in this work. The ERA5 data have been obtained from the Copernicus Climate Data Store (CDS).

Data availability statement. The CLARA-A3 documentation consists of an Algorithm Theoretical Basis Document (ATBD), Validation Report (VAL) and Product User Manual (PUM), all available online on the webpage `https://doi.org/10.5676/EUM_SAF_CM/CLARA_AVHRR/V003`, which also contains hyperlinks to the CM SAF Web User Interface (WUI) where the actual data can be freely downloaded.

APPENDIX A

RSF processing error (regional uncertainty) during pre-CERES era (1979-1999)

Three typical orbital configurations (defining observational temporal coverage of the diurnal cycle) exist in the pre-CERES (1979-1999) period of the data record: morning-only, afternoon-only, and morning+afternoon. Each of these three configurations is mimicked using a selection of CERES-era satellites which are equivalent in terms of ECT during limited time periods, an overview of which is provided in Table A1.

Subsequently, daily and monthly mean RSF data are generated for each of the three typical orbital configurations, each using its own associated selection of (CERES-era) satellites and limited time periods. From this, the average processing error (MAB) for each typical orbital configuration is calculated (last two columns in Table A1). Since we know the orbital configuration is the largest source of error, these numbers provide an estimate of the processing error during the pre-CERES era.

Hence, it is now possible to “fill” the gap in the entire data record’s accuracy time series, i.e. extending the lower panel in Figure 5 to the upper panel.

Orbital config.	**Pre-CERES (1979-1999) orbital configuration**		**CERES-era (2000-2020) equivalent orbital configuration (similar local ECT**)**			
	Satellite (*)	**Duration (months)**	**Satellite***	**Duration**	**MAB (W/m^2)**	
					MM	**DM**
(I) Afternoon satellite only	T-N N-7 N-7 N-9 N-9	1979/01-1980/01: 13 1981/09-1983/08: 24 1984/06-1985/01: 08 1985/02-1985/06: 05 1985/11-1986/10: 12 ***Total: 62 months***	N-16 N-18 N-19	2005/01-2006/12 2012/01-2013/12 2016/01-2017/12	Range: 4.1 - 6.3 Mean: **4.8** <8 (100%) <4 (0%) <2 (0%)	Range: 10.6 - 19.1 Mean: **13.5** <16 (88.7%) <8 (0%) <4 (0%)
(II) Morning satellite only	N-6 N-12	1980/02-1981/08: 19 1994/09-1994/12: 04 ***Total: 23 months***	N-15 N-15 N-16 N-18	2000/03-2000/07 2001/03-2001/06 2011/01-2011/12 2017/07-2018/06	Range: 5.2 - 8.6 Mean: **6.6** <8 (84.8%) <4 (0%) <2 (0%)	Range: 13.2 - 23.1 Mean: **17.4** <16 (35.3%) <8 (0%) <4 (0%)
(III) Afternoon and morning satellite only	N-7/-8 N-9/-8 N-9/-10 N-11/-10 N-11/-12 N-14/-12 N-14/-15	1983/09-1984/05: 09 1985/07-1985/10: 04 1986/11-1988/10: 24 1988/11-1991/09: 35 1991/10-1994/08: 35 1995/01-1998/11: 47 1998/12-2000/02: 15 ***Total: 169 months***	N-14/-15 N-15/-16 N-16/-18 N-18/-19	2001/03-2001/07 2004/01-2005/12 2011/01-2011/12 2017/07-2018/06	Range: 2.3 - 6.3 Mean: **3.6** <8 (100%) <4 (73.6%) <2 (0%)	Range: 6.7 – 19.0 Mean: **10.4** <16 (99.2%) <8 (15.7%) <4 (0%)
(*) T=TIROS, N=NOAA; (**) Equator Crossing Time						

TABLE A1. Estimation of RSF uncertainty during pre-CERES era.

References

Akkermans, T., and N. Clerbaux, 2020: Narrowband-to-broadband conversions for top-of-atmosphere reflectance from the Advanced Very High Resolution Radiometer (AVHRR). *Remote Sensing*, **12 (2)**, 305.

Akkermans, T., and N. Clerbaux, 2021: Retrieval of Daily Mean Top-of-Atmosphere Reflected Solar Flux Using the Advanced Very High Resolution Radiometer (AVHRR) Instruments. *Remote Sensing*, **13 (18)**, 3695.

Canty, T., N. Mascioli, M. Smarte, and R. Salawitch, 2013: An empirical model of global climate–part 1: A critical evaluation of volcanic cooling. *Atmospheric Chemistry and Physics*, **13 (8)**, 3997–4031.

Clerbaux, N., T. Akkermans, E. Baudrez, A. Velazquez Blazquez, W. Moutier, J. Moreels, and C. Aebi, 2020: The Climate Monitoring SAF Outgoing Longwave Radiation from AVHRR. *Remote Sensing*, **12 (6)**, 929.

CMSAF, 2021: CDOP-3 Product Requirements Document. Document SAF/CM/DWD/PRD v3.8, EUMETSAT Satellite Application Facility on Climate Monitoring (CM SAF), Offenbach, Germany. Available online at: ftp://gerb.oma.be/tomakker/CLARA_A3/SAF_CM_DWD_PRD_3_8.pdf.

CMSAF, 2022: Validation Report for Top-of-atmosphere products from the CMSAF Cloud, Albedo, Radiation data record, AVHRR-based, Edition 3 (CLARA-A3). Document SAF/CM/RMIB/VAL/GAC/TOA Issue 1.1, EUMETSAT Satellite Application Facility on Climate Monitoring (CM SAF), Offenbach, Germany. Available online at: https://www.cmsaf.eu/SharedDocs/Literatur/document/2023/saf_cm_rmib_val_gac_toa_1_1_pdf.html.

Doelling, D. R., and Coauthors, 2013: Geostationary enhanced temporal interpolation for CERES flux products. *Journal of Atmospheric and Oceanic Technology*, **30 (6)**, 1072–1090.

Ellingson, R. G., H.-T. Lee, D. Yanuk, and A. Gruber, 1994: Validation of a technique for estimating outgoing longwave radiation from HIRS radiance observations. *Journal of Atmospheric and Oceanic Technology*, **11 (2)**, 357–365.

Hersbach, H., and Coauthors, 2020: The ERA5 global reanalysis. *Quarterly Journal of the Royal Meteorological Society*, **146 (730)**, 1999–2049.

Hogan, R. J., and A. Bozzo, 2018: A flexible and efficient radiation scheme for the ECMWF model. *Journal of Advances in Modeling Earth Systems*, **10 (8)**, 1990–2008.

Johnson, G. C., J. M. Lyman, and N. G. Loeb, 2016: Improving estimates of Earth's energy imbalance. *Nature Climate Change*, **6 (7)**, 639–640.

Karlsson, K.-G., and Coauthors, 2013: CLARA-A1: a cloud, albedo, and radiation dataset from 28 yr of global AVHRR data. *Atmospheric Chemistry and Physics*, **13 (10)**, 5351–5367.

Karlsson, K.-G., and Coauthors, 2017: CLARA-A2: the second edition of the CM SAF cloud and radiation data record from 34 years of global AVHRR data. *Atmospheric Chemistry and Physics*, **17 (9)**, 5809–5828.

Karlsson, K.-G., and Coauthors, 2023a: CLARA-A3: CM SAF cLoud, Albedo and surface RAdiation dataset from AVHRR data - Edition 3. Satellite Application Facility on Climate Monitoring (CM SAF), URL https://wui.cmsaf.eu/safira/action/viewDoiDetails?acronym=CLARA_AVHRR_V003, https://doi.org/10.5676/EUM_SAF_CM/CLARA_AVHRR/V003.

Karlsson, K.-G., and Coauthors, 2023b: CLARA-A3: the third edition of the AVHRR-based CM SAF climate data record on clouds, radiation, and surface albedo covering the period 1979 to 2023. *submitted to: Earth System Science Data (ESSD).*

Lee, H., C. Schreck, and K. Knapp, 2014: Generation of the daily OLR climate data record. *2014 EUMETSAT meteorological satellite conference*, 22–26.

Lee, H.-T., A. Gruber, R. G. Ellingson, and I. Laszlo, 2007: Development of the HIRS outgoing longwave radiation climate dataset. *Journal of Atmospheric and Oceanic Technology*, **24 (12)**, 2029–2047.

Loeb, N. G., B. A. Wielicki, D. R. Doelling, G. L. Smith, D. F. Keyes, S. Kato, N. Manalo-Smith, and T. Wong, 2009: Toward optimal closure of the Earth's top-of-atmosphere radiation budget. *Journal of Climate*, **22 (3)**, 748–766.

Loeb, N. G., and Coauthors, 2018: Clouds and the earth's radiant energy system (CERES) energy balanced and filled (EBAF) top-of-atmosphere (TOA) edition-4.0 data product. *Journal of Climate*, **31 (2)**, 895–918.

Stengel, M., and Coauthors, 2020: Cloud_cci Advanced Very High Resolution Radiometer post meridiem (AVHRR-PM) dataset version 3: 35-year climatology of global cloud and radiation properties. *Earth System Science Data*, **12 (1)**, 41–60.

Wielicki, B. A., B. R. Barkstrom, E. F. Harrison, R. B. Lee III, G. L. Smith, and J. E. Cooper, 1996: Clouds and the Earth's Radiant Energy System (CERES): An earth observing system experiment. *Bulletin of the American Meteorological Society*, **77 (5)**, 853–868.

Young, A. H., K. R. Knapp, A. Inamdar, W. Hankins, and W. B. Rossow, 2018: The international satellite cloud climatology project H-Series climate data record product. *Earth System Science Data*, **10 (1)**, 583–593.

Zhang, Y., W. Rossow, A. Lacis, and V. Oinas, 2019: Calculation, evaluation and application of long-term, global radiative flux datasets at ISCCP: past and present. *Study of cloud and water processes in weather and climate through satellite observations Submitted for. World Scientific Publishing Company as the second volume in a multi-part series on Earth sciences*.